Noname manuscript No.
(will be inserted by the editor)

Rate of change of J-integral in creep-fatigue condition

Abhishek Tiwari

Received: date / Accepted: date

Abstract The operational conditions in next generation power plants and other high temperature applications such as turbine blades in jet engines demand the component to perform under extreme conditions where metallic materials show time dependent deformation under cyclic loading conditions. Under creep-fatigue loading condition, the crack tip is exposed to both time dependent and independent plastic deformation. Conventional crack characterizing parameters such as $(\mathrm{C}_t)_{,avg}$ has shown good correlation with dominant damage based crack velocity, $(\mathrm{d}a/\mathrm{d}t)_{avg}$. However, the true definition or prediction of crack driving forces under such scenario are vague due to limited theoretical validity of the conventional crack tip characterizing parameters, such as J or C_t. In this work, the concept of configurational forces are applied for the first time to understand the creep-fatigue crack growth behaviour. The crack growth is simulated using node-release technique and the configurational forces are calculated using post processing the finite element results for calculation of dJ/dt.

Keywords configurational forces, creep-fatigue crack, node release, crack driving force

1 Introduction

Aero turbine engines, steam headers and components of future Advanced Ultra Super Critical power plants operate under cyclic loading conditions at elevated temperatures. For these components, life prediction is of utmost importance for the safety and maintenance of the machinery as well as lives associated with it. Under creep-fatigue loading, the damage near the crack tip is both due to the cyclic plastic deformation as well as time dependent creep deformation.[1] reported on his work on Cr-Mo-V steel that for a high yield strength material, the unloading stage in creep-fatigue loading does not resharpen the crack and the stresses are not reinstated due to cyclic plasticity.[1] also explained that as creep deformation is not fully reversed by the cyclic plasticity, the creep zone expands with continuous loading/unloading to the extent that the fatigue driven crack growth is negligible. With continued cyclic loading the the rate of expansion of creep zone also becomes sluggish and the overall crack growth rate can decrease below the crack growth rate without creep.[2] also found in his study on alloy 709 that the creep dominated crack growth was minimum and there was no significant difference between crack growth rate due to fatigue and creep-fatigue for a holding time of 60s as well as 600s.[3] and[4] have analysed and described the complete, partial and no creep reversal category of the materials for a crack under creep-fatigue condition.

The conventional crack tip characterizing parameters, such as, $(C_t)_{\mathrm{avg}}$ appears to be describing the crack growth per unit cycle for various metallic material such as ferritic/martensitic steels, stainless steels, super-alloys etc.[1;4;3]. However, there are two different models for measuring $\mathrm{d}a/\mathrm{d}N$. One adds the crack growth due to cyclic loading and due to creep whereas, the other takes the dominant step and hence known as dominant damage model. Although, the crack tip stress field is shown to be described by C_t-integral under creep deformation, it cannot describe the true crack driving force[5]. Due to this reason the potential to describe true crack driving force by $(C_t)_{\mathrm{avg}}$ parameter is also questionable. The theory of integral like C_t and $C^\star$ are based

Corresponding Author: Abhishek Tiwari
Department of Metallurgical and Materials Engg., Indian Institute of Technology Ropar, Punjab, India

on Hoff's analogy which can only work as long as strain rate is a sole function of stress. However, this is not the case under small scale creep where elastic strains are significantly high.

In order to answer some of the questions related to the true crack driving forces under creep-fatigue condition, the concept of configurational forces are applied. The advantage of this concept is that it is independent of materials' constitutive response and hence can describe the true crack driving force. The J-integral calculated using the concept of configurational forces is valid for materials deforming under creep and fatigue. This work is a first attempt to apply this concept in creep-fatigue condition and the recent studies on the application of configurational forces in creep crack growth by [5] and [6] has shown that the rate of change of J-integral calculated using the concept of configurational forces are path independent in the small scale creep conditions at the crack tip, unlike C_t and $C^\star$ integrals.

In this article, the concept and validity window of $C^\star$ integral is described which is followed by the crack tip characterizing parameters under creep-fatigue condition. Consequently, the concept of configurational forces in brief is described and its application in creep fatigue condition is worked out in the subsequent section. The numerical analysis using commercial finite element software Abaqus [7] is carried out on a compact tension specimen using node release technique and a trapezoidal wave form of creep-fatigue loading to understand the crack driving forces in creep-fatigue crack extension.

2 Crack tip characterization in presence of time dependent deformation

In a material under steady-state creep conditions, creep strain rate, $\dot{\varepsilon_c}$ and stresses are related by a power-law expression,

$$\dot{\varepsilon_c} = A \cdot \sigma^n, \tag{1}$$

where n denotes the creep exponent and A denotes the creep coefficient. In a component with a crack, Small Scale Creep (SSC) condition persists when the creep zone is confined to a small region near the crack tip, surrounded by an elastic field that is characterized by the stress intensity factor K (or the J-integral J). Extensive creep (EC) conditions prevail, if the creep zone extends through the whole ligament of the body. The intermediate stage between SSC and EC is called transition creep (TC) conditions [4].

The important point as a difference in extensive creep and SSC is not the size of zone but the comparative creep strains and elastic strains. In EC, the creep strains are significantly higher than the elastic strains and therefore, Hoff's analogy [8] of replacing strain with strain rate in J-integral to arrive at a similar C*-integral works. However, in SSC, because elastic strains are also significantly high, the total strain is not only a function of stress but stress rate as well and therefore, the Hoff's analogy cannot be used to arrive at an integral similar to J.

If steady-state creep condition engulfs the whole ligament of the body, the C*-integral has been defined in analogy to the J-integral as path-independent line integral [9;10;11] as,

$$C^\star = \int_\Gamma (\dot{\phi} \mathrm{d}y - \mathrm{T_i} \frac{\partial \dot{u_i}}{\partial x}) \mathrm{d}s. \tag{2}$$

In Eq. (2), Γ denotes a contour around the crack tip with ds as increment of the contour line, T is the traction vector, $\dot{u_i}$ is the displacement rate vector, and $\dot{\phi}$ is the strain energy density rate. The C*-integral determines the stresses and strain rates near the crack tip in a form analogous to the HRR-field equations.

[4] derived another similar integral which can be easily measured, experimentally, and is found by separating the time independent and time dependent displacements. This integral also known as C$_t$ integral is described as,

$$C_t = \frac{1}{B} (\frac{\partial}{\partial a} \int_0^{\dot{\Delta}_t} P \mathrm{d}\dot{\Delta}_t), \tag{3}$$

where a is the crack length, B is the thickness of the specimen, $\dot{\Delta}_t$ is the rate of change of time dependent displacement or creep displacement and P is the constant force which is applied on the specimen.

3 Crack tip characterization under creep-fatigue condition

Under creep fatigue loading condition, usually a waveform loading is applied comprising of a loading part or rise time (t_r), a hold part (t_h) and an unloading part or decay time (t_d). Different loading forms have been experimentally and numerically investigated in the literature [12;13;14]. The crack tip characterizing parameter in case of creep-fatigue loading is $(\mathrm{C_t})_{\mathrm{avg}}$ which was proposed by [4]. For the limiting cased of creep strain complete and no reversal, the $(\mathrm{C_t})_{\mathrm{avg}}$ is calculated as described in Eq.(4).

The two extreme cases are following:

- No creep reversal: The cyclic plasticity does not reinstate or redistribute the stresses. No creep strain is reversed in the unloading part of the cyclic loading.

– Complete creep reversal: In this case all the creep strain accumulated during hold period is reversed during unloading.

A third category also exists, in which partial creep reversal takes place. For the two limiting cases, the crack growth characterization parameter, $(C_t)_{,avg}$, is described as follows.

$$(C_t)_{,avg} = \frac{1}{t_h}\int_{(N-1)t_h}^{Nt_h} C_t \mathrm{d}t, \tag{4a}$$

$$(C_t)_{,avg} = \frac{1}{t_h}\int_{(0}^{t_h} C_t \mathrm{d}t, \tag{4b}$$

The process of finding the crack tip characterization parameter found in [4;15;2;1] is also followed in this work and the same is explained briefly in this section. The crack growth per unit cycle, $\mathrm{d}a/\mathrm{d}N$, has been used in [15] and [2] as,

$$(\frac{\mathrm{d}a}{\mathrm{d}N}) = (\frac{\mathrm{d}a}{\mathrm{d}N})_L + (\frac{\mathrm{d}a}{\mathrm{d}N})_H, \tag{5}$$

where L and H subscripts denote the crack growth per unit cycle due to cyclic and creep deformations, respectively. The $(\mathrm{d}a/\mathrm{d}N)_L$ is calculated using Paris's law with consideration to opening stress intensity factor as,

$$(\frac{\mathrm{d}a}{\mathrm{d}N})_L = A \cdot (\Delta K_{eff})^B, \tag{6}$$

where ΔK_{eff} is calculated as,

$$(\Delta K_{eff}) = (K_{\max} - K_{\mathrm{op}}), \tag{7}$$

where, K_{op} is the stress intensity factor at a load where the crack mouth is open, i.e. crack opening displacement (COD) is just >0. Important fact to consider here is that load at which COD is just >0 initially increased in the work of [15] attributed to the plastic wake and then saturated after 20-30 nodes were released. This amount of node release is equivalent to 0.4 to 0.6mm.

The stress intensity factors are calculated as per [16]. The crack growth per unit cycle for creep deformation is calculated as,

$$(\frac{\mathrm{d}a}{\mathrm{d}N})_H = \frac{\mathrm{d}a}{\mathrm{d}t}_H \cdot t_H, \tag{8}$$

where, $(\frac{\mathrm{d}a}{\mathrm{d}t})_H$ is the crack growth velocity during the hold period and t_H is the hold time. [15] has used an empirical correlation to calculate the value of $(\frac{\mathrm{d}a}{\mathrm{d}t})_H$, however, this can also be calculated directly from the simulation results by measuring the crack growth and then dividing by the hold time.

[4] has mentioned a dominant damage formulation for calculation of $(\frac{\mathrm{d}a}{\mathrm{d}N})$, which appears to be better and is calculated by giving preference to the dominant mechanism by which the crack extension occurs. This is calculated as,

$$(\frac{\mathrm{d}a}{\mathrm{d}N}) = max[(\frac{\mathrm{d}a}{\mathrm{d}N})_L, (\frac{\mathrm{d}a}{\mathrm{d}N})]_H. \tag{9}$$

In this work, dominant damage i.e. Eq.(9) is used for comparing the crack driving force parameters as no difference in the values were found between dominant damage and conventional da/dN formula.

The $(C_t)_{,\mathrm{avg}}$ value are calculated experimentally as,

$$(C_t)_{,\mathrm{avg}} = \frac{P_{\max}(\Delta \dot{V}_C))}{(BB_N)^{1/2} W t_H}(\frac{f'}{f}), \tag{10}$$

where ΔV_C is the difference in the load line displacement at the beginning and the end of the hold period of the creep step in the creep-fatigue wave (see Fig. 1).

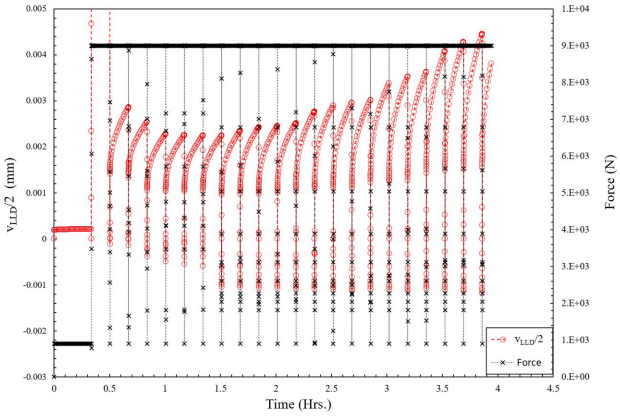

Fig. 1 Load line displacement ($v_{LLD}/2$) obtained as a response from the simulation for an applied trapezoidal waveform loading scheme shown in Fig. 3.

Factor $\frac{f'}{f}$ is the ratio of derivative of specimen geometry function f and f, which for Compact Tension (CT) specimen is described as per ASTM E2670 as,

$$f = [\frac{2 + a/W}{(1 - a/W)^{3/2}}](0.886 + 4.64(a/W) - 13.32(a/W)^2 + 14.72(a/W)^3 - 5.6(a/W)^4. \tag{11}$$

4 Configurational forces in creep-fatigue condition

Configurational forces usually arise when there is a defect in the material due to non-zero value of divergence of the Eshelby's energy-momentum tensor [17;18;19;20]. In

simple words, if there is a spatial change (material inhomogeneity) in the mechanical response of the material a configurational force will arise at the boundary where the transition in the mechanical response takes place in reference configuration. These are also known as material forces and extensive study on the calculation and theory of configurational forces in fracture mechanics and in presence of other material inhomogeneities has been performed in recent years [21;22;23;24;20;6].

In a homogeneous elastic plastic material under small strain assumption, the total strain is composed of elastic and plastic parts. The strain energy density is symbolized with ϕ, where only the elastic part of the strain energy density, ϕ_e, is recoverable. As J-intgeral was developed assuming non-linear elasticity (NLEL), the total strain energy density assuming NLEL will be comprising of ϕ_e, ϕ_{pl} and ϕ_C, where subscript 'pl' denotes instantaneous plasticity and 'C' denotes time dependent creep behavior. In a homogeneous material the bulk configurational forces are described as,

$$\mathbf{f} = -\nabla \cdot (\phi \mathbf{I} - \mathbf{F}^{\mathrm{T}} \mathbf{S}) \tag{12}$$

where, $\mathbf{F}^{\mathrm{T}}$ is the transpose of the deformation gradient and $\mathbf{S}$ is the first Piola-Kirchhoff Stress tensor. The divergence is represented by ∇ and identity tensor by $\mathbf{I}$, respectively.

The $\mathbf{J}-$integral is calculated by adding the configurational forces in a contour Γ around the crack tip. The scalar value of $\mathbf{J}-$integral is found by taking the $\mathbf{J}$ vector's projection in the expected crack extension direction, i.e.,

$$J = \mathbf{e} \cdot \int_{\Gamma} \mathbf{f} \cdot dl, \tag{13}$$

where $\mathbf{e}$ denotes the unit vector in the direction of crack extension and dl is a line element of Γ[??]. In Eq.(12), if ϕ is replaced with ϕ_e, the configurational forces obtained in such case represent the elastic plastic behaviour and hence the configurational forces are denoted as f_{ep}. The J$-$integral in this case is also denoted as J$_{ep}$. If NLEL condition is assumed and ϕ includes elastic, plastic as well as creep strain energy densities, then J-integral is denoted as J$_{nlel}$.

Hoff's analogy, as discussed briefly earlier, makes it possible to arrive at a contour integral $C^{\star}$, where strain is replaced with strain rate and displacement with displacement rate. However, the definition of crack driving force in this integration is lost because $C^{\star}$ can only be valid when strain is a function of stress only, i.e. under extensive creep condition and due to this dominance of creep strain under such assumption, elastic strain energy density rate is not counted in the integral. As we know that only elastic energy is available for the crack to drive, a better characterization may be by finding the derivative of $J-$ integral with time. One should also note that $C^{\star}$ or similar integrals are not equal to $\mathrm{d}J/\mathrm{d}t$ and therefore, these integrals do not represent the rate of change of crack driving force. $C^{\star}$ or similar integrals are important in extensive creep conditions and these integrals do describe the stress distribution near the crack tip.

By taking advantage of the concept of configurational forces which are independent of any constitutive response of materials, $J-$integral can be calculated without having any theoretical anomaly. In an elastic-plastic material deformation, the deformation gradient $\mathbf{F}$ comprises of elastic and plastic components, $\mathbf{F}^{\mathrm{e}}$ and $\mathbf{F}^{\mathrm{p}}$, respectively. The elastic strain energy density is a function of $\mathbf{F}^{\mathrm{e}}$ only. The bulk configurational forces, $\mathbf{f}$ appear in the plastically deforming region as $\mathbf{f^{ep}}$ is a function of gradient of plastic strain described by [24] as,

$$\mathbf{f^{ep}} = \boldsymbol{\sigma} \cdot \frac{\partial \boldsymbol{\varepsilon}_{\mathbf{pl}}}{\partial \boldsymbol{X}}, \tag{14}$$

where, $\mathbf{X}$ represents the spatial positions in reference configuration, and $\boldsymbol{\varepsilon}_{\mathrm{pl}}$ represents the plastic strain. The details of the derivations and significance of plastic strain on calculation of J_{ep} is provided in [21;24].

Due to the dependency of configurational forces on plastic strains, the J_{ep} is path dependent for any contour which lies inside the plastic zone or creep zone. However, for a contour encompassing the plastic/creep zone, J_{ep} would be equal to the J_{ep} calculated for any other contour outside plastic/creep zone including the remote contour defined as J_{far}, i.e. path independent.

In a material which deforms under creep conditions, the total strain can be dissociated into elastic strain, $\varepsilon_{\mathrm{el}}$ and creep strain, $\varepsilon_{\mathrm{cr}}$. In such scenario, the creep strain is analogous to plastic strain in terms of the affect it has on bulk configurational forces. The bulk configurational forces in this case would correspond to,

$$\mathbf{f^{ep}} = \boldsymbol{\sigma} \cdot \frac{\partial \boldsymbol{\varepsilon}_{\mathbf{cr}}}{\partial \boldsymbol{X}}, \tag{15}$$

where $\varepsilon_{\mathrm{cr}}$ is the creep strain. Therefore, the same understanding, which is described for the case of elastic-plastic material deformation can be extrapolated here by stating that the J_{ep} would be path independent for any contour outside the creep zone.

The configurational forces are calculated using Eq. (12) using both NLEL assumption and using only elastic energy rate density for $\mathbf{f}_{\mathrm{nlel}}$ and $\mathbf{f}_{\mathrm{ep}}$. The J-integral from configurational forces are calculated by summing the bulk configurational forces in the expected crack extension direction. More details on calculation of configurational forces can be found in the appendix of [17].

5 Numerical simulation of Creep Fatigue crack growth (CFCG) of Mod-P91 steel at 625^oC

[15] has investigated CFCG both experimentally and numerically on austenitic stainless steel alloy (Alloy 709) at 600 and 700^{o}C and modified 9Cr-1Mo (Mod-P91) steel at 625^{o}C. The CFCG tests were performed by [15] on Mod-P91 steel specimens of 12.5mm thickness and the same geometry is modelled for characterization of crack tip parameters and crack growth velocity using node release technique, in this work. In his work, it was found that the crack opening load, i.e. the force values, where crack opening displacement is > 0, increased with increase in crack depth and this behaviour saturated after approximately 20 node release. The loading cycle wave form which [15] used and which is also used in this study is shown in Fig. 1, schematically.

The CT specimen modelled in this work is 50mm wide and 12.5mm thick with an initial crack length to width ratio of 0.5. Node release technique is used to simulate crack growth. One node is released after each cycle for initial four cycles, 2 nodes for next 4 cycles, 3 nodes for another 4 cycles, 4 nodes for 4 more cycles, 5 nodes for next 3 cycles and 6 nodes for next 4 cycles. This scheme is used and implemented in Abaqus using python script to obtain a varying da/dN and da/dt values. The loading time in each cycle of 0.1677Hrs is 2 secs, with a hold period of 600 sec followed by an unloading step of 2 secs. Linear quadratic plane strain elements are used for half symmetric two dimensional model with reduced integration. The element size was kept constant at the cracked area for calculation ease (see [20] and to avoid irregularities due to discretization error at the crack tip (for discretization error in configurational forces see [21]). The element size is 0.1x0.1mm^2. The mesh of the CT specimen and magnified view at the crack tip is shown in Fig.5 (a) and (b), respectively.

Exhaustive studies have been performed on the path independence of the $J-$integral calculated from configurational forces by [17;21;6;20]. It has been found in these studies that as long as the deformation zone is contained in the contour, the line integral remains path independent. Path dependencies arise in elastic-plastic (also for elastic creep) configurational forces when a contour passes through a deformation zone (plastic zone or creep zone). This is a problem for calculation of configurational force based $J-$integral under excessive creep condition where C_t and similar integrals show path independence. In small and medium scale creep where C_t and $C^\star$ integrals are path dependent, rate of change of configurational force based $J-$integral has shown path independence [6;5]. Keeping this in mind two contours were defined for calculations of all types of

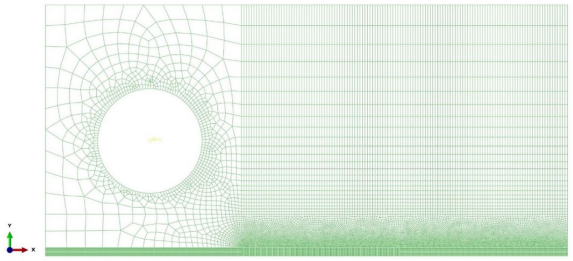

(a) Mesh of CT specimen

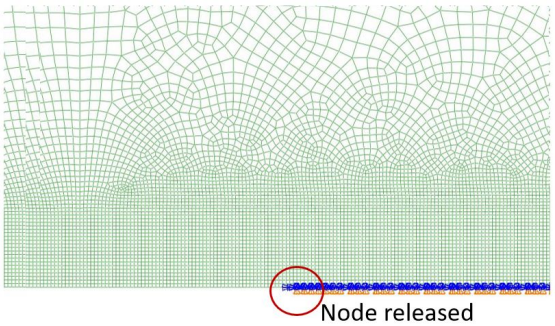

(b) Mesh at the crack tip

Fig. 2 Linear quadrilateral plane strain reduced integration elements in half symmetric 2D CT specimen for simulation crack extension using node release technique.

line integrals. First contour is 7mm high along the y-axis, 10mm in x-direction from the initial crack tip and 4mm on the back side of the initial crack tip. This contour denoted as Γ_{10}. Another contour remains on the boundary of the specimen excluding one node along the boundary and only 4mm on the back side from the initial crack tip to avoid the influence of loading pin hole of the CT specimen. This contour is denoted as Γ_{far}.

The material properties used for simulating the modified P-91 steel at 625^o C is taken from literature [15;4] and is listed in Table 1.

Table 1 Material properties used in FE simulation of mod-P91 at 625^o C

E [GPa]	**v**	σ_o [MPa]	σ_{uts} [MPa]	**A** [MPa$^{-2.4}Hr^{-1}$]	**n**
125	0.3	325	344	3.55E-07	2.4

6 Results

6.1 Behaviour of opening load and COD

For the loading scheme shown in Fig. 3, the load line displacement, v_{LLD}, is calculated from the center of the pin which was connected with the pin hole surface of the CT specimen using kinematic coupling. The boundary condition in the simulation except the node release is explained in [25].

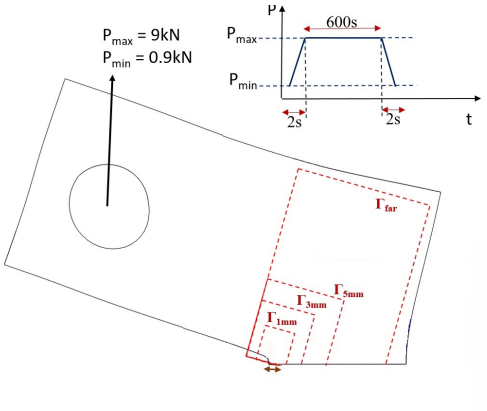

Fig. 3 Schematic half symmetric CT specimen with the creep-fatigue load cycle and the contours used for J and C_t integral calculations.

The v_{LLD} is plotted in Fig. 1 along with the force values. The v_{LLD} values as shown in Fig. 1 is not positive at the beginning of the loading cycle. This trend is similar to the finding of [15]. The P_{op} values calculated corresponding to the positive v_{LLD} in the beginning of the loading cycle and was confirmed by the COD value >0, measured manually in each step at a node just ahead of the instantaneous crack tip. The normalized P_{op} values with P_{max} is plotted along with the [15] data in Fig. 4.

It is evident from Fig. 4 that the trend of P_{op} found in the simulation of this work joins the trend of [15] simulation. The simulations of [15] and that in this work have a few differences. The plastic properties used in [15] were defined as ideal plastic behaviour with σ_o equals to the average of σ_o and σ_{uts} listed in table 1. Second difference is that the $\mathrm{d}a/\mathrm{d}N$ and $\mathrm{d}a/\mathrm{d}t$ values are simulated differently in this work which differ from the range of $\mathrm{d}a/\mathrm{d}N$ and $\mathrm{d}a/\mathrm{d}t$ in the work of [15]. In this work, the plastic behaviour is simulated with a linear interpolation from σ_o to σ_{uts} to avoid convergence problems due to ideal plastic constraints and a better representation of metal plasticity.

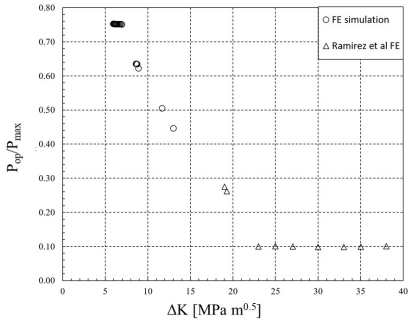

Fig. 4 Normalized opening force vs ΔK compared with [15] finding.

6.2 Creep and plastic zone sizes

The plastic zone and creep zone sizes are measured from the simulation manually and has been shown in Fig. 6.2 and 6. For all the crack growth values the plastic zone size is smaller than the creep zone except in the initial stage when creep starts developing after application of load. The creep zone size progressively increases and engulfs the whole ligament whereas the plastic zone size remains more or less unaltered. This result confirms the scenario of no creep reversal and hence, Eq.(16b) is used for $(\mathrm{C}_t)_{\mathrm{avg}}$ calculation. It also makes us expect that the initial condition will be small scale creep where C_t integral must be path dependent. In such case the question arises that C_t value corresponding to which contour should be used for calculating $(\mathrm{C}_t)_{\mathrm{avg}}$. In our calculation, C_t value corresponding to 10mm contour is used for $(\mathrm{C}_t)_{\mathrm{avg}}$ calculation as the energy close to the crack tip describes the energy available to the crack. In configurational force based $\mathrm{d}J/\mathrm{d}t$ calculation, this problem does not arise as $\mathrm{d}J/\mathrm{d}t$ shows path independent behavior in the small scale creep condition (for more details on path independence of $\mathrm{d}J/\mathrm{d}t$ see [5] and [6]).

6.3 $(C_t)_{\mathrm{avg}}$ and $\mathrm{d}J/\mathrm{d}t$

Similar to the crack growth per unit cycle [4] has proposed calculation of crack growth rate using dominant damage mechanism as well. The conventional and dominant damage based crack growth rates are calculated as,

$$(\frac{\mathrm{d}a}{\mathrm{d}t})_{,avg} = \frac{1}{t_{\mathrm{h}}}[(\frac{\mathrm{d}a}{\mathrm{d}N}) - (\frac{\mathrm{d}a}{\mathrm{d}N})_{\mathrm{o}}], \tag{16a}$$

$$(\frac{\mathrm{d}a}{\mathrm{d}t})_{,avg} = \frac{1}{t_{\mathrm{h}}}[(\frac{\mathrm{d}a}{\mathrm{d}N})], \tag{16b}$$

In our calculation, no difference if dominant damage or conventional method of calculation for da/dt (using

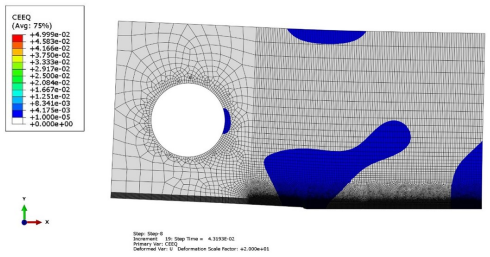

zone.jpg

(a) Creep zone size

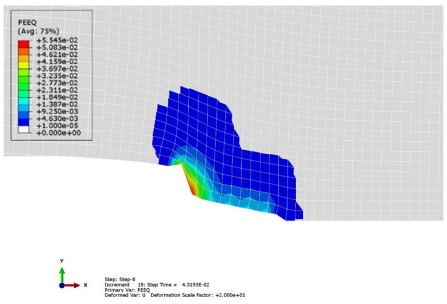

(b) Plastic zone size

Fig. 5 Equivalent plastic strain and creep strain representing the size of the respective deformation zones for a crack extension of 1mm (t = 1.46 Hrs).

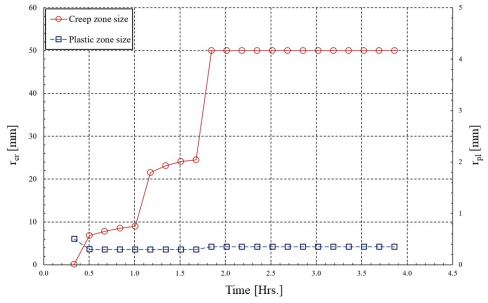

Fig. 6 Plastic zone radius and creep zone radius measured manually at the end of each set of node release.

Eq.(16) or da/dN (using Eq.(5)) and Eq.(9) is found. The plot comparing $(da/dt)_{\text{avg}}$ vs $(C_t)_{\text{avg}}$ for two different sets of modified P91 specimens for 600s hold time for a trapezoidal waveform taken from the work of[4] (Chapter 9) is compared with the data generated by numerical simulation in this work on mod-P91 steel using node release technique. The data of[15] is also compared in Fig. 6.3 (a). In Fig. 6.3 (b) $(C_t)_{\text{avg}}$ values for aforementioned data-sets are compared along da/dN.

In Fig. 6.3 (a), it can be seen that Saxena's sets are showing different trend from that of[15] data and our simulation data which are very close to each other. However, a huge scatter is observed in mod-P91 dataset at 625^{o}C for 600s hold period in other literature as well (for instance see[26]) which show different trend in different da/dt regions. The reason for such a huge scatter for an event which is not as probabilistic as ductile to brittle transition region[27;28] is not completely known or mentioned in the literature. One reason could be the path dependency of C$_t$-integral in small scale creep. It is redundantly proven in recent studies by[6;5] that dJ/dt shows path independent behaviour in small and medium scale scale creep unlike C$_t$-integral and hence, dJ/dt can be a better approach to reduce the scatter.

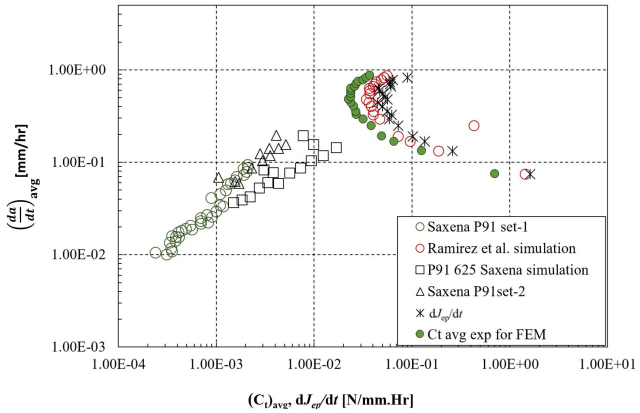

(a) $(C_t)_{\text{avg}}$ vs $(da/dt)_{\text{avg}}$

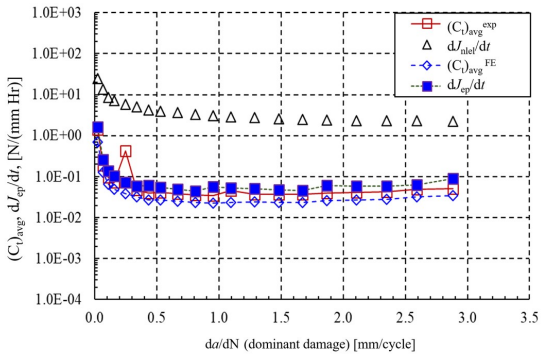

(b) (da/dN) vs $(C_t)_{\text{avg}}$

Fig. 7 Comparative behaviour of crack tip parameters such as $(C_t)_{\text{avg}}$, dJ_{ep}/dt, dJ_{nlel}/dt at different crack growth rates.

7 Summary and Outcomes

Following major outcome are found in this work.

– With our quest to describe the true crack driving force and to describe the small scale creep condition in creep fatigue crack growth, Fig. 6.3 (b) clearly shows that dJ_{ep}/dt is not far from the $(C_t)_{\text{avg}}$ and therefore, in case of path dependent behaviour of

C_t-integral question may arise to choose the right contour for $(C_t)_{\text{avg}}$ calculation. This problem can be avoided by using dJ_{ep}/dt.
- C_t-integral although defines the stress field at the crack tip, it lacks any relation with the crack driving force as it does not describe the rate of change of J-integral. The true crack driving force can be obtained only by counting the elastic strain energy rate density as only elastic energy is available for crack extension. Therefore, dJ_{ep}/dt describes the rate of change of true crack driving force.
- As the J_{ep} is obtained by configurational force approach, both J_{ep} and dJ_{ep}/dt are independent of material's constitutive response and therefore can be used in crack extension and cyclic loading conditions without any theoretical invalidation unlike conventional J-integral.

Further, one can notice that the conventional J-integral which assumes the material to be non-linear elastic (shown in Fig. 6.3 as dJ_{nlel}/dt) is much larger than all other parameters. This also shows that even though, C_t-integral uses both elastic and creep strain energy rate density, the behavior is closer to dJ_{ep}/dt rather than dJ_{nlel}/dt. The reason could be that the elastic strains are very high in the small scale creep regime and the strain energy rate density is not much influenced by the creep energy rate density (Φ_{cr}). Under extensive creep condition, the rate of change of elastic strain energy density is similar to that of creep strain energy density.

In this work, the plastic zone is always smaller than the creep zone and hence, the behaviour of $(C_t)_{\text{avg}}$ will be different when complete or significant creep reversal happens, which is not in the present scope of this work.

Acknowledgements

This work was supported by the ISIRD Phase 1 funding from Indian Institute of Technology Ropar, Punjab, India. The author acknowledges the support from the Institute.

Compliance with ethical standards

Conflicts of interest/Competing interests

The authors have no conflicts of interest to declare that are relevant to the content of this article.

Data Availability statement

The authors confirm that the data supporting the findings of this study are available within the article and in[15].

References

1. Adefris N, Saxena A, McDowell D. Creep-fatigue crack growth behavior in 1Cr-1Mo-0.25 V steels. Part I: estimation of crack tip parameters. Fatigue & Fracture of Engineering Materials & Structures. 1996;19(4):387–398.
2. Shaber N, Stephens R, Ramirez J, Potirniche GP, Taylor M, Charit I, et al. Fatigue and creep-fatigue crack growth in alloy 709 at elevated temperatures. Materials at High Temperatures. 2019;36(6):562–574.
3. Grover P, Saxena A. Modelling the effect of creep-fatigue interaction on crack growth. Fatigue & fracture of engineering materials & structures. 1999;22(2):111–122.
4. Saxena A. Advanced fracture mechanics and structural integrity. CRC Press; 2019.
5. Kolednik O, Tiwari A, Posch C, Kegl M. Configurational force based analysis of creep crack growth. International Journal of Fracture. 2022;p. 1–25.
6. Tiwari A. Effect of material inhomogeneity under creep and plastic to creep transition of cracks. Procedia Structural Integrity. 2022;39:290–300.
7. Abaqus G. Abaqus 6.18. Dassault Systemes Simulia Corporation, Providence, RI, USA. 2018;.
8. Hoff NJ. Approximate analysis of structures in the presence of moderately large creep deformations. Quarterly of Applied Mathematics. 1954;12(1):49–55.
9. Landes J, Begley J. A Fracture Mechanics Approach to Creep. In: Mechanics of Crack Growth: Proceedings of the Eighth National Symposium on Fracture Mechanics, a Symposium. vol. 10. ASTM; 1976. p. 128.
10. Ohji K, Ogura K, Kubo S. Creep crack propagation rate in SUS 304 stainless steel and interpretation in terms of modified J-integral. Trans Jpn Soc Mech Eng. 1976;42:350–358.
11. Nikbin K, Webster G, Turner C. Relevance of nonlinear fracture mechanics to creep cracking. In: Cracks and fracture. ASTM International; 1976. .
12. Saxena A. Fracture mechanics approaches for characterizing creep-fatigue crack growth. JSME international journal Ser A, Mechanics and material engineering. 1993;36(1):1–20.

13. Tanaka K. Creep–fatigue crack propagation in lead-free solder under cyclic loading with various waveforms. Engineering fracture mechanics. 2010;77(11):1750–1762.
14. Plumtree A, Yu MT. INFLUENCE OF HOLD TIMES ON THE HIGH TEMPERATURE FATIGUE CRACK PROPAGATION RATE. In: Mechanical Behaviour of Materials V. Elsevier; 1988. p. 1013–1019.
15. Ramirez J, Potirniche GP, Shaber N, Taylor M, Pugesek H, Stephens R, et al. The influence of plasticity-induced crack closure on creep-fatigue crack growth in two heat-resistant steels. International Journal of Fatigue. 2019;125:291–298.
16. E2760 A. Standard Test Method for Creep-Fatigue Crack Growth Testing. ASTM, Annual Book of Standards. 2019;.
17. Kolednik O, Kasberger R, Sistaninia M, Predan J, Kegl M. Development of damage-tolerant and fracture-resistant materials by utilizing the material inhomogeneity effect. Journal of Applied Mechanics. 2019;86(11).
18. Maugin GA. Configurational forces: thermomechanics, physics, mathematics, and numerics. CRC Press; 2016.
19. Gurtin ME. The nature of configurational forces. In: Fundamental Contributions to the Continuum Theory of Evolving Phase Interfaces in Solids. Springer; 1999. p. 281–314.
20. Tiwari A, Wiener J, Arbeiter F, Pinter G, Kolednik O. Application of the material inhomogeneity effect for the improvement of fracture toughness of a brittle polymer. Engineering Fracture Mechanics. 2020;224:106776.
21. Kolednik O, Schöngrundner R, Fischer FD. A new view on J-integrals in elastic–plastic materials. International Journal of Fracture. 2014;187(1):77–107.
22. Simha N, Fischer F, Kolednik O, Chen C. Inhomogeneity effects on the crack driving force in elastic and elastic–plastic materials. Journal of the Mechanics and Physics of Solids. 2003;51(1):209–240.
23. Simha N, Fischer FD, Kolednik O, Predan J, Shan G. Crack tip shielding or anti-shielding due to smooth and discontinuous material inhomogeneities. International journal of fracture. 2005;135(1):73–93.
24. Simha N, Fischer FD, Shan G, Chen C, Kolednik O. J-integral and crack driving force in elastic–plastic materials. Journal of the Mechanics and Physics of Solids. 2008;56(9):2876–2895.
25. Tiwari A, Avinash G, Sunil S, Singh R, Ståhle P, Chattopadhyay J, et al. Determination of reference transition temperature of In-RAFMS in ductile brittle transition regime using numerically corrected Master Curve approach. Engineering Fracture Mechanics. 2015;142:79–92.
26. Narasimhachary S, Saxena A. Crack growth behavior of 9Cr- 1Mo (P91) steel under creep–fatigue conditions. International Journal of Fatigue. 2013;56:106–113.
27. Tiwari A, Gopalan A, Shokry A, Singh R, Ståhle P. Fracture study of ferritic/martensitic steels using Weibull stress analysis at quasi-static and higher loading rates. International Journal of Fracture. 2017;205(1):103–109.
28. Tiwari A, Singh R. Fracture behaviour of ferritic/martensitic steels in DBT region characterized using CT and TPB specimen geometries. International Journal of Fracture. 2018;209(1):241–249.